

# Angular momentum generation in cold gravitational collapse

D. Benhaïem<sup>1</sup>, M. Joyce<sup>2,3</sup>, F. Sylos Labini<sup>4,1,5</sup> and T. Worrakitpoonpon<sup>6</sup>

<sup>1</sup> Istituto dei Sistemi Complessi Consiglio Nazionale delle Ricerche, Via dei Taurini 19, 00185 Rome, Italy

<sup>2</sup> UPMC Univ Paris 06, UMR 7585, LPNHE, F-75005, Paris, France

<sup>3</sup> CNRS IN2P3, UMR 7585, LPNHE, F-75005, Paris, France

<sup>4</sup> Centro Studi e Ricerche Enrico Fermi, Via Panisperna 89 A, Compendio del Viminale, 00184 Rome, Italy

<sup>5</sup> INFN Unit Rome 1, Dipartimento di Fisica, Università di Roma Sapienza, Piazzale Aldo Moro 2, 00185 Roma, Italy

<sup>6</sup> Faculty of Science and Technology, Rajamangala University of Technology Suvarnabhumi, Nonthaburi Campus, Nonthaburi 11000, Thailand

Received / Accepted

**Abstract.** During the violent relaxation of a self-gravitating system a significant fraction of its mass may be ejected. If the time varying gravitational field also breaks spherical symmetry this mass can potentially carry angular momentum. Thus starting initial configurations with zero angular momentum can in principle lead to a bound virialized system with non-zero angular momentum. We explore here, using numerical simulations, how much angular momentum can be generated in a virialized structure in this way, starting from configurations of cold particles which are very close to spherically symmetric. For initial configurations in which spherical symmetry is broken only by the Poissonian fluctuations associated with the finite particle number  $N$ , with  $N$  in range  $10^3$  to  $10^5$ , we find that the relaxed structures have standard “spin” parameters  $\lambda \sim 10^{-3}$ , and decreasing slowly with  $N$ . For slightly ellipsoidal initial conditions, in which the finite- $N$  fluctuations break the residual reflection symmetries, we observe values  $\lambda \sim 10^{-2}$ , of the same order of magnitude as those reported for elliptical galaxies. The net angular momentum vector is typically aligned close to normal to the major semi-axis of the triaxial relaxed structure, and also with that of the ejected mass. This simple mechanism may provide an alternative, or complement, to “tidal torque theory” for understanding the origin of angular momentum in astrophysical structures.

**Key words.** methods: numerical; galaxies: elliptical and lenticular, cD; galaxies: formation

## 1. Introduction

Observations have shown already several decades ago that galaxies of all types generically have significant angular momentum. Its origin remains a fascinating open theoretical problem (for a review, see e.g. Romanowsky & Fall (2012)). Globular clusters have also been more recently observed to have net rotation (Hénault-Brunet et al., 2012; Bellazzini et al., 2012; Kacharov et al., 2014). The most popular theory to account for angular momentum in virialized structures is so-called “tidal torque theory” in which the virialized structure gains angular momentum by the action of the torque due to the tidal fields generated by surrounding structures (Peebles, 1969). We explore here a distinct mechanism which, despite its simplicity, appears not to have been considered in the literature, apart from in one recent study of cold spherical collapse by one of us (Worrakitpoonpon, 2015): generation of angular momentum by ejection of

matter in violent relaxation. Indeed violent relaxation of self-gravitating structures is characterized by very large amplitude variations of the mean field potential of a structure, which can give enough energy to particles to escape even if all the mass is initially bound. The amount of mass ejected depends strongly on the initial conditions, varying from zero to as much as 40% for highly uniform and completely cold initial conditions (Joyce, Marcos & Sylos Labini, 2009)<sup>1</sup>. If, in addition, the mass distribution is not spherically symmetric during the violent phase of the relaxation, this ejected mass would be expected to carry at least some angular momentum — and “generate” in the remaining bound mass an (equal and opposite) amount of angular momentum. In other words the two components of the mass — the part that is ejected, and the other part which remains bound — can exert a net torque on one another during the violent relaxation leading to a net angular momentum

<sup>1</sup> Mergers of virialized structures can also lead to ejection of a significant mass, in particular when the two structures have very different mass (Carucci et al., 2014).

for both of them. Further, given that violent relaxation starting from a wide range of cold initial conditions is often characterized by a very strong breaking of spherical symmetry even when the initial conditions are not — leading in particular to triaxial relaxed structures (e.g. Merritt & Aguilar (1985); Barnes, Lanzel & Williams (2009); Benhaïem & Sylos Labini (2015); Sylos Labini, Benhaïem & Joyce (2015)) — one might expect the effect to be far from negligible.

We explore here, using numerical simulations, how much angular momentum can be generated in a virialized structure by this mechanism. More specifically we consider an isolated initially cold distribution of matter in open boundary conditions, and without expansion, and a range of initial spatial distributions which are very close to spherically symmetric: (i) particles distributed around a center following a mean density profile which decays as a power law of the radial distance, or (ii) particles distributed with uniform mean density inside an ellipsoidal region. These are initial conditions which have been extensively studied in the literature (see references below) to investigate the processes involved in the formation of galaxies and other astrophysical structures. We note that, in a cosmological context, the simulations can be taken to represent the evolution, in physical coordinates, of a single isolated overdensity with the chosen initial profile. On the other hand the relation of such simulations to the more general case of the evolution an overdensity in an expanding universe (which cannot necessarily be well approximated as isolated) is a more complex issue, and will be discussed in detail in a separate forthcoming publication. It involves several additional parameters which can play a role in the dynamics (e.g. how precisely the background density is modelled) and additional numerical issues (notably concerning the control of numerical accuracy without energy conservation, see Joyce & Sylos Labini (2012); Sylos Labini (2012)).

In the present context the fluctuations breaking spherical symmetry in the initial conditions are evidently of central importance for the phenomenon we are studying. In the first case spherical symmetry is broken only by the finite particle number fluctuations, while in the second case these fluctuations break the residual reflection symmetries. We find that almost all these initial conditions — except where there is negligible mass ejection — indeed lead to a measurable net angular momentum in the relaxed virialized structure. The magnitude of this angular momentum is larger by about an order of magnitude in the latter class, and in many cases is sufficiently large to suggest that the mechanism could potentially account for angular momenta observed in astrophysical structures. Indeed, the typical measured values of the spin parameters of galaxies (see e.g. Hernandez et al. (2007)) are of the same order of magnitude as those we find in our simulations.

The paper is organized as follows. We first present the details of the numerical simulations and initial conditions in Sect.2. In the following section we then present our re-

sults, first describing the relevant features of the evolution qualitatively and then giving the quantitative results. In Sect.4 we summarize our results and conclude.

## 2. Numerical simulations

### 2.1. Initial conditions

In detail the initial conditions of which we study the evolution are the following:

- $N$  particles distributed *randomly* inside a sphere of radius  $R_0$ , following the radius-dependent density profile  $\rho(r) \propto r^{-\alpha}$  where  $r$  is the radial distance from the centre and  $\alpha$  is a constant. We will refer to these as “spherical initial conditions”. The particles have vanishing initial velocities. We report here results for the range of  $\alpha$  with  $0 \leq \alpha \leq 2$ . We restrict to this range as in a previous study (Sylos Labini, 2012; Sylos Labini, Benhaïem & Joyce, 2015) we have observed that, for  $\alpha > 2$ , there is negligible ( $\ll 1\%$ ) mass ejection. As shown in this same study, the evolution leads, except for  $\alpha$  very close to zero, to virial equilibria which are very non-spherically symmetric, and typically triaxial. We have varied the number of particles  $N$  from  $10^3$  to  $10^5$ .
- $N$  particles are distributed randomly in a prolate ellipsoidal region. We define  $a_3$  to be the largest semi-principal axis and  $a_1 = a_2$  the smaller ones. The three eigenvalues of the inertia tensor are simply

$$\Lambda_i = \frac{1}{5}M(a_j^2 + a_k^2) \quad (1)$$

where  $M$  is the total mass of the system, and  $i \neq j \neq k$  and  $i, j, k = 1, \dots, 3$ : from the definition of the semi-principal axes we have  $\Lambda_1 \geq \Lambda_2 \geq \Lambda_3$ . Note that the principal axis corresponding to the eigenvalue  $\Lambda_1$  is oriented in the direction of the shortest semi-principal axis  $a_1$ , while the principal axis associated with  $\Lambda_3$  is in the direction of the longest one  $a_3$ . The particle number  $N$  spans again the range from  $10^3$  to  $10^5$ .

The shape at any time may then be characterized by the parameter <sup>2</sup>

$$\iota(t) = \frac{\Lambda_1(t)}{\Lambda_3(t)} - 1. \quad (2)$$

We will refer to these as “ellipsoidal initial conditions”, and report here results for value of  $\iota$  in the range from  $\iota(0) = 0.01$  to  $\iota(0) = 0.25$ . The mass ejection and amplification of the spherical symmetry breaking during the evolution from these initial conditions has been studied in Benhaïem & Sylos Labini (2015).

<sup>2</sup> Note that these parameters are generally defined as a function of the semi-principal axes  $a_1, a_2, a_3$  rather than as a function of the eigenvalues (see Eq.1). However for small deformations of a perfect sphere, which is the case we consider here, these definitions are almost equivalent. The advantage of this definition of the parameters using the eigenvalues is that it can be used to characterize any distribution.

## 2.2. Numerical simulations

We have used the N-body code **Gadget** (Springel, 2005). All results presented here are for simulations in which energy is conserved to within *one tenth of a percent* over the time scale evolved, with maximal deviations at any time of less than half a percent (see Benhaïem & Sylos Labini (2015); Sylos Labini, Benhaïem & Joyce (2015) for more details). This accuracy has been attained using values of the essential numerical parameters in the **Gadget** code [0.025 for the  $\eta$  parameter controlling the time-step, and a force accuracy of  $\alpha_F = 0.001$ ] in the range of typically used values for this code. In the specific cases of spherical initial conditions with  $\alpha = 0$ , which is singular in the limit  $N \rightarrow \infty$ , the treatment is as detailed in Joyce, Marcos & Sylos Labini (2009) (see also Worrakitpoonpon (2015)). We have also performed extensive tests of the effect of varying the force smoothing parameter  $\varepsilon$ , and found that we obtain very stable results provided it is significantly smaller than the minimal size reached by the whole structure during collapse<sup>3</sup>. We will discuss the dependence on particle number  $N$  of our results below.

As noted above, our simulations are performed with open boundary conditions and in a non-expanding background, but can be taken to represent well the evolution of an isolated overdensity in an expanding universe, which, at the initial time, is of high density compared to the mean mass density of the universe and at rest, in physical or comoving coordinates. In this respect we could perform the simulations here using the expanding universe version of the code and periodic boundary conditions. The size of the periodic box relative to that of the initial sphere would then fix the relative overdensity represented by the sphere at the initial time (and thus also the time scale for virialization compared to the Hubble time). Such a simulation gives, as discussed in detail and studied at length in Joyce & Sylos Labini (2012); Sylos Labini (2012), identical results in physical coordinates, modulo finite size corrections suppressed by the ratio of the size of the structure to the size of the periodic box, and possible numerical effects (including the effect of smoothing). Indeed, as discussed in Joyce & Sylos Labini (2012); Sylos Labini (2012), the differences between such simulations and those in open non-expanding space provides information about such numerical effects, and indeed a tool to control better expanding universe simulations. Our “direct” simulations in physical coordinates are preferable because they are simpler and, notably, far easier to control for accuracy (via energy conservation).

Given that we are interested here in the angular momentum, we also test our simulations for its overall conservation and, as detailed below, compare the measured angular momentum of the final bound structure with the

numerical error. We will also check systematically for the accuracy of conservation of the total linear momentum.

## 3. Results

### 3.1. Qualitative description of mechanism

Numerical studies of evolution from some of these initial conditions, or very similar ones with small but non-zero virial ratios, have been reported extensively in the literature (see e.g. Henon (1973); van Albada (1982); Aarseth, Lin & Papaloizou (1988); Theis & Spurzem (1999); Boily, Athanassoula & Kroupa (2002); Joyce, Marcos & Sylos Labini (2009); Sylos Labini (2012, 2013); Benhaïem & Sylos Labini (2015); Sylos Labini, Benhaïem & Joyce (2015)), with an emphasis in particular on the study of the shape and profile of the virialized structure. Because the system is initially cold it undergoes in all cases a strong collapse, in a time of order  $1/\sqrt{G\rho_0}$  where  $\rho_0$  is the initial mean density, followed by a re-expansion which leads rapidly to virialization of most of the mass. The “degree of violence” of the collapse — which can be characterized roughly by the maximal contraction the system undergoes — varies with the initial condition. The most extreme case is the spherical case ( $\alpha = 0$ ) in which the collapse is singular in the limit  $N \rightarrow \infty$ .

While both early studies, and most studies since then, have focused on the properties of the virialized structure (e.g. its density profile, shape, and velocity distributions) the phenomenon of mass (and energy) ejection has been considered in detail only more recently: for the case of cold uniform spherical conditions (i.e. the case  $\alpha = 0$  here) in Joyce, Marcos & Sylos Labini (2009), for the case  $\alpha = 0$  with non-zero initial velocities in Sylos Labini (2012) and for ellipsoidal initial conditions in Benhaïem & Sylos Labini (2015)<sup>4</sup>. Essentially the amount of mass ejected depends on the degree of violence of the relaxation, which can be quantified roughly by the maximal contraction attained by the system during the collapse phase. The reason for this correlation between the ejection of mass and the violence of collapse becomes easy to understand when the mechanism for ejection is studied (Joyce, Marcos & Sylos Labini, 2009; Carucci et al., 2014; Benhaïem & Sylos Labini, 2015; Sylos Labini, Benhaïem & Joyce, 2015): The ejected particles are essentially those of which the fall times to the center of the structure during collapse are longest. As a consequence they pass through the center of the whole structure when it has begun re-expanding, which means that they travel into a deeper potential than the one that they travel out of. As a result they pick up an energy “kick”. The magnitude of this energy gain is directly related to the strength of the potential at this time, which depends essentially on the extent of the contraction.

<sup>3</sup> More specifically we have found very stable results for  $\varepsilon$  in the range  $R_g^{min}/\varepsilon \in [10, 200]$  where  $R_g^{min}$  is the minimal value of the gravitational radius (defined further below) reached during the collapse.

<sup>4</sup> Mass ejection in mergers of two virialized structures is studied in detail in Carucci et al. (2014); Samsing (2015).

For the generation of angular momentum, the second crucial ingredient, in addition to mass ejection, is the breaking of spherical symmetry. Indeed mass ejection can occur in a purely radial gravitational field, but will not then generate angular momentum. That cold initial conditions in the class we are considering lead to virialized states that are very far from spherically symmetric was observed first by Merritt & Aguilar (1985), and extensively studied in the literature (see e.g. Aguilar & Merritt (1990); Theis & Spurzem (1999); Boily & Athanassoula (2006); Barnes, Lanzel & Williams (2009)). This instability of initially spherical systems to relaxation to non-spherical viral equilibria is usually referred to as “radial orbit instability”, because of its apparent link to an instability of equilibrium systems with purely radial orbits originally proved by Antonov (1961); Fridman et al. (1984). In two recent papers we have studied in detail the development of this asymmetry during the collapse phase for both the classes of initial conditions we study in this paper (spherical initial conditions in Sylos Labini, Benhaïem & Joyce (2015), and ellipsoidal initial conditions in Benhaïem & Sylos Labini (2015)). These studies reveal that the same process involved in the energy ejection leading to mass ejection plays a crucial role, for many initial conditions, in amplifying the symmetry breaking. Indeed, amongst the late arriving particles, there is also a spread in arrival times as a function of angle, which leads to an energy injection, and thus a spatial distribution of mass, which is also a function of angle. The effect is maximal in enhancing the final asymmetry in the range  $\alpha \in [0.5, 1.5]$ . It is, on the other hand, relatively suppressed in the limit  $\alpha = 0$  because the particles’ fall times, and consequently their energy changes, are much less strongly correlated with their initial radial position in this case, leading to a “washing out” of the effect. The development of the asymmetry in the mass distribution, and thus in the gravitational potential, is the combined result of the growth of the initial finite  $N$  fluctuations breaking spherical symmetry through gravitational instability — known in this case as the Lin, Mestel & Shu (1965) instability — which is then amplified by the energy ejection to particles which also leads to mass ejection.

A schematic representation of the mechanism is given in Figure 1. Any given realization of our initial conditions has a longest semi-principal axis, along which particles are on average further from the orthogonal plane. In the case of the spherical initial conditions the non-zero effective ellipticity is a finite  $N$  effect, while in the ellipsoidal initial conditions it is dialed by the parameter  $\iota(0)$ . In the first phase of collapse this initial asymmetry is amplified by the (gravitational) instability of Lin, Mestel & Shu (1965) with the collapse occurring latest along the longest axis. Particles arriving from the corresponding directions pass through the center as the structure is already re-expanding in the other directions, leading to a greater energy injection to them. As the potential they are traveling is not spherically symmetric the particles also gain traverse velocities and thus angular momenta with respect to the

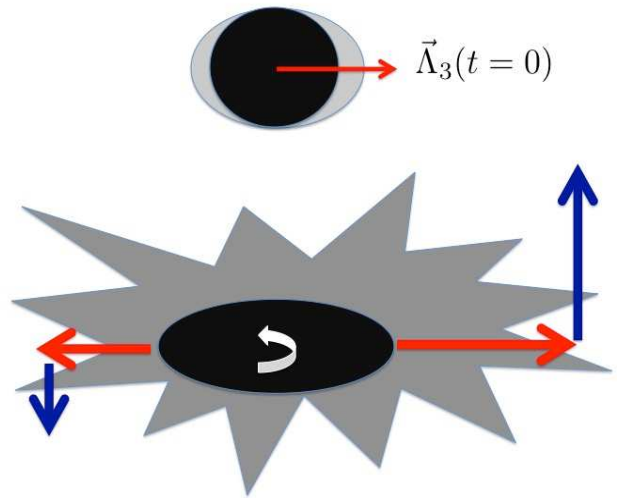


**Fig. 1.** Schematic representation of the generation of angular momentum in the ejected particles. The upper panel shows schematically symmetry breaking in the initial cloud. When particles are ejected both their radial and traverse components will generally have some dependence on angle, leading to a net angular momentum being carried away by the ejected particles.

center. As there are also fluctuations breaking rotational symmetry, which grow in the course of the collapse, both the radial and transverse velocities will vary as a function of direction, and, for example, those ejected in opposite directions will have slightly different angular momentum. The ejected outgoing particles can then carry net non-zero angular momentum leaving behind the opposite angular momentum in the particles which virialize in the bound structure.

### 3.2. Measurement of angular momentum

We now focus on the evolution of the angular momentum during the relaxation. More specifically we decompose the total angular momentum  $\mathbf{L}_T$  at any time into two components:

$$\mathbf{L}_T = \mathbf{L}_b + \mathbf{L}_f \quad (3)$$

where  $\mathbf{L}_b$  ( $\mathbf{L}_f$ ) is the total angular momentum of the “bound” (“free”) particles, i.e., which have negative (positive) energy at the given time. In practice particles’ energies almost never change sign more than once, i.e., the asymptotically ejected particles are those which are tagged as “free” when their energy becomes positive. Further we consider the decomposition of  $\mathbf{L}_b$  as

$$\mathbf{L}_b = \mathbf{L}_b^{com} + \mathbf{L}_b^p \quad (4)$$

where  $\mathbf{L}_b^{com} = M_b \mathbf{R}_b \times \mathbf{V}_b$  is the angular momentum of the center of mass, located at  $\mathbf{R}_b$  and moving with velocity  $\mathbf{V}_b$ , of the bound particles, and  $\mathbf{L}_b^p$  is the angular



momentum of the bound particles with respect to their center of mass. It is the latter which interests us here primarily, but we also monitor  $\mathbf{L}_b^{com}$  and  $\mathbf{L}_T$ , measured with respect to the fixed origin at the center of mass of the initial configuration, to assess the accuracy of the simulation for which the total angular momentum should be conserved (and equal to zero).

We will measure time in units of

$$\tau_c = \sqrt{\frac{3\pi}{32G\bar{\rho}_0}} \quad (5)$$

where  $\bar{\rho}_0$  is the total initial mass density, i.e., the total mass divided by the volume of the initial sphere or ellipsoid. It corresponds to the time for a particle initially at the outer periphery of a cold sphere with this mass density to fall to its center in the continuum approximation, (i.e. taking  $N \rightarrow \infty$  and keeping the initial mass density profile fixed) and without shell crossing.

We will measure angular momentum in the natural units given by

$$L_0 = \frac{GM^{5/2}}{\sqrt{|E_0|}} \quad (6)$$

where  $M$  is the total (initial) mass of the system, and  $E_0$  its total (initial) energy (equal to its potential energy). Further, we will report results for the angular momentum of the bound mass  $\mathbf{L}_b^p$  given in terms of the so-called “spin parameter”  $\lambda$  as defined by Peebles (1969); Knebe & Power (2008):

$$\lambda = \frac{|\mathbf{L}_b^p|}{L_0^b} \quad (7)$$

where  $L_0^b$  is

$$L_0^b = \frac{GM_b^{5/2}}{\sqrt{|E_b|}} \quad (8)$$

where  $M_b$  is the bound mass and  $E_b$  ( $W_b$ ) the total (gravitational potential) energy of this mass (with respect to its center of mass)<sup>5</sup>.

### 3.3. Results for a chosen initial condition

We present results first for the case of spherical initial conditions with  $\alpha = 1$ , and  $N = 10^5$  particles. We consider this case as its evolution is typical of what we observe for all our different initial conditions. The panels of Fig.2 show for this case, as a function of time, (i) the fraction  $f_+$  of the initial mass in free particles, and the gravitational radius defined as  $R_g(t) = \frac{GM_b^2(t)}{|W_b(t)|}$ , (ii) the flattening ratio  $\iota_{80}$  as defined by (2), with the subscript indicating that the inertia tensor is calculated using the particles with energy

<sup>5</sup> Another commonly used normalization for the spin is that introduced in Bullock et al. (2001), defined by  $\lambda' = |\mathbf{L}_b^p|/L_1$  with  $L_1 = \sqrt{2M_b^3GR_b}$  with  $R_b = -\frac{3GM_b^2}{5W_b}$  where  $W_b$  is the potential energy. For a virialized structure, with  $E_b = W_b/2$ ,  $\lambda' = \sqrt{5/3}\lambda$ .

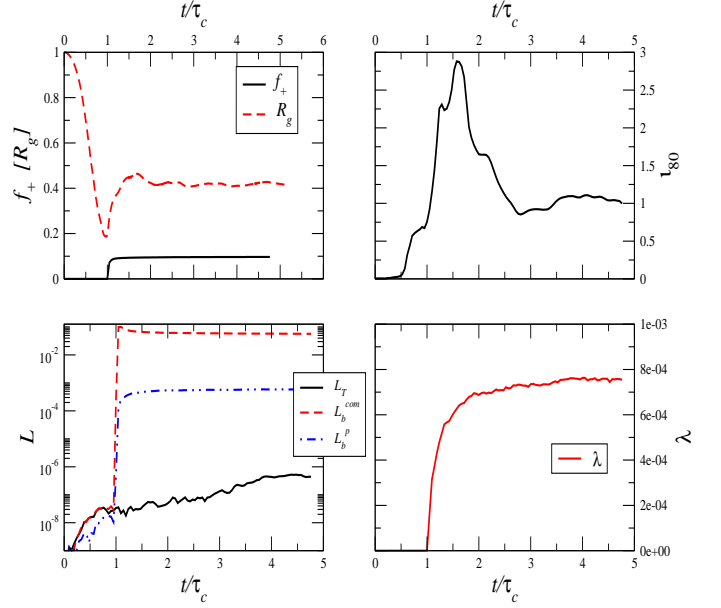


**Fig. 2.** Evolution from spherical initial condition with  $\alpha = 1$ , and  $N = 10^5$ : (top left) the fraction of particles with positive energy  $f_+$  (full black line) and the gravitational radius  $R_g$  (dotted red line) in units of the initial sphere radius  $R_0$ ; (top right) the flatness ratio  $\iota_{80}$  for the 80% most bounded particles; (bottom left) the total angular momentum  $L_T$  (full black line) with respect to the initial center of mass, the angular momentum of the center of mass of the bound particles  $L_b^{com}$  (red dashed line) and the angular momentum of the bound particles  $L_b^p$  (blue dashed-dotted line) with respect to their center of mass (all in units of  $L_0$  defined in Eq. 6); (bottom right) the spin parameter  $\lambda$ .

less than 20 % of the energy of the most bound particle, (iii) the magnitude of the angular momenta  $|\mathbf{L}_T|$ ,  $|\mathbf{L}_b^{com}|$ ,  $|\mathbf{L}_b^p|$  (on a logarithmic scale), and (iv) the spin parameter  $\lambda$ .

The first plot illustrates clearly, as described above, that at  $\tau_c \approx 1$ , the system reaches its maximal contraction, and the strong energy injection which leads to particle ejection occurs in a very short interval around this time, corresponding approximately to the dispersion in fall times of the mass. Likewise we see in the second plot, showing the behavior of  $\iota_b$ , that the breaking of spherical symmetry grows monotonically from the beginning and is then strongly amplified around the maximal collapse by the energy injection (as described in detail in Sylos Labini, Benhaïem & Joyce (2015)).

As anticipated, as can be seen from the lower two plots, the bound mass indeed goes toward a stationary state with non-zero angular momentum (relative to its center of mass). This final angular momentum of the bound mass, albeit small in the natural units, is clearly not numerical in origin: it is about three orders larger than the fi-

nal total angular momentum which gives a measure of the violation of angular momentum conservation due to numerical error. Further we have performed several tests varying the essential numerical parameters and found our results to be stable. On the other hand the total angular momentum  $\mathbf{L}_b$  of the bound mass (with respect to the initial center of mass of the whole system) is dominated by its translational motion: the bound mass “recoils” with a net linear momentum compensating that of the ejected mass, along an axis which is off-set from the initial center of mass. We will give some further details below on this ejected linear momentum, which is measured numerically to a precision of order  $10^{-6}$  (i.e. the measured momentum change of these particles is  $10^6$  times larger than the change in the total momentum due to numerical error).

### 3.4. Generation of angular momentum during collapse

It is interesting to follow the dynamics leading to the generation of the ejection of net angular momentum in the collapse phase. During this phase the mass which gets ejected has not yet undergone the energy boost which leads to its ejection, but the gravitational potential has already developed very significant asymmetry which leads the particles to have non-radial velocities, and thus non-zero angular momentum (while the total angular momentum remains zero).

Shown in Fig.3 is, again for the case  $\alpha = 1$  and  $N = 10^5$ , the measured dispersion of the transverse velocities in radial shells, as a function of radius, and at different times during the evolution. The velocity is normalized in units of  $v_0 = \sqrt{GM/R_0}$ . We observe that the transverse velocities are already, at  $t = 0.5\tau_c$  comparable with, and, at  $t = 0.75\tau_c$ , even larger than their magnitude in the final virialized structure. Note that these are the transverse velocities produced by the growth of the initial density fluctuations breaking spherical symmetry through gravitational instability, well before the energy injection to particles arriving around  $t \approx \tau_c$  which leads to the mass (and angular momentum) ejection. At longer time scales, i.e.  $t > \tau_c$ , the outer shell, corresponding to very weakly bound particles with energy very close to zero, is still expanding as these particles are still traveling outward on their large orbits. On the other hand the inner shell has reached a stationary state, as can be seen by comparing the number density profiles at  $t = 2.5\tau_c$  and at  $t = 5\tau_c$ .

In Fig.4 is shown the distribution  $P(|\ell|)$  of the absolute values of the particle angular momentum  $\ell$  with respect to the center of mass of bound particles, at a few different indicated times (before and after the collapse). We observe, in line with the results on the transverse velocities, that significant angular momentum is generated already before the completion of the collapse phase. Further for  $t > \tau_c$   $P(|\ell|)$  rapidly approaches the distribution characterizing the final virialized state.

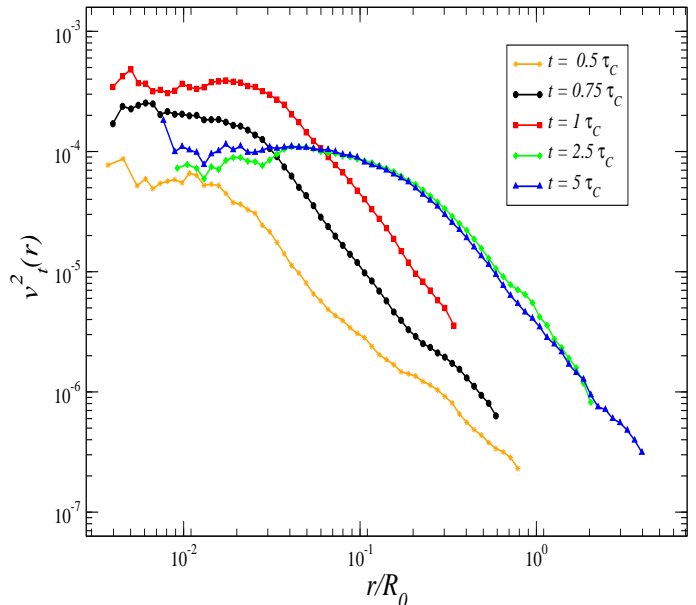


**Fig. 3.** Average in radial shells of the square of the transverse component of particle velocities (in units in which  $v_0 = \sqrt{GM/R_0}$  is unity), as a function of radius, at each of the indicated times, for a simulation with  $N = 10^5$  particles of spherical initial conditions with  $\alpha = 1$ . Note that already well before the system reaches its maximal contraction, at  $t \approx 1$ , the Poissonian fluctuations breaking spherical symmetry have been amplified to produce tangential velocities larger than in the final virialized state.

Shown in the upper panel of Figure 5 is the temporal evolution of the average value of the modulus of the particle angular momentum, for the bound particles (with respect to their center of mass, in units of  $L_0$ ). In line with what would be expected from the plots of the transverse velocities, we observe a constant growth during the collapse phase, followed by a very significant boost around the time of maximal contraction, when the energy ejection occurs. Thus we see the angular momentum generated by the collapse receives a very significant boost in the final phase of the collapse. This is further quantified by the lower panel of Figure 5 which shows the evolution, as a function of time, of

$$l_b^p = \frac{L_b^p}{\sum_i |\ell|_i} \quad (9)$$

i.e. the modulus of the angular momentum of bound particles, normalized to the sum of the moduli of the angular momenta of the same particles. The dashed horizontal line corresponds to the value  $\sqrt{N_+/N_-} \approx f_+/\sqrt{N}$ , which is the amplitude of the bound angular momentum which would be expected if the ejection operated as a simple random removal of particles without any modification of their angular momentum. We observe that the final value is in fact at least several times larger. Thus, during the final

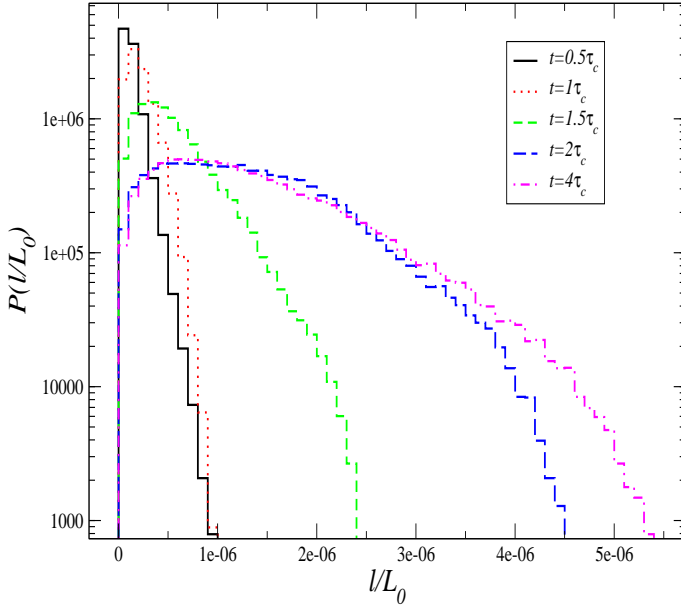


**Fig. 4.** Distribution of the absolute values of the particle angular momentum  $\ell$  (in units of  $L_0$ ) with respect to the center of mass of bound particles  $P(|\ell|)$ , for  $\alpha = 1$  and  $N = 10^5$  at different times before and after the collapse.

phase of collapse in which the large energy changes giving rise to ejection occur, the ejected and bound particles exert a torque on one another which very significantly amplifies their final (equal and opposite) angular momenta.

### 3.5. Results for different initial conditions (fixed $N$ )

In the above we have focused, for simplicity, on the single case of spherical initial conditions with  $\alpha = 1$ , and we have shown results for  $N = 10^5$ . The qualitative behaviors we have discussed in this case, for what concerns the generation of angular momentum, are shared by all our other initial conditions. Quantitatively there is a variation of the final angular momentum, which depends notably on the details of the mass ejection and the degree of symmetry breaking during the collapse. The precision of the simulations also varies from case to case — simulations for the spherical initial conditions with  $\alpha = 0$  are particularly delicate as the collapse is the most extreme in this case, with a singular behavior in the limit  $N \rightarrow \infty$ . Correspondingly in this case the measured angular momentum is only a few times larger than the numerical error in the conservation of the total angular momentum, while it is, as shown above (see Fig. 2) almost three orders of magnitude for the case  $\alpha = 1$ .

Fig. 6 shows the “final” values of  $f_+$  (top panel),  $\iota_{80}$  (third panel) and  $\lambda$  (bottom panel), i.e. at  $t = 5\tau_c$ , for the spherical initial conditions as a function of  $\alpha$ . In addition, in the second panel, is shown also  $f_E$ , the “fraction of ejected energy”, defined by  $f_E = (E_b - E_0)/E_0 = -E_p/E_0$

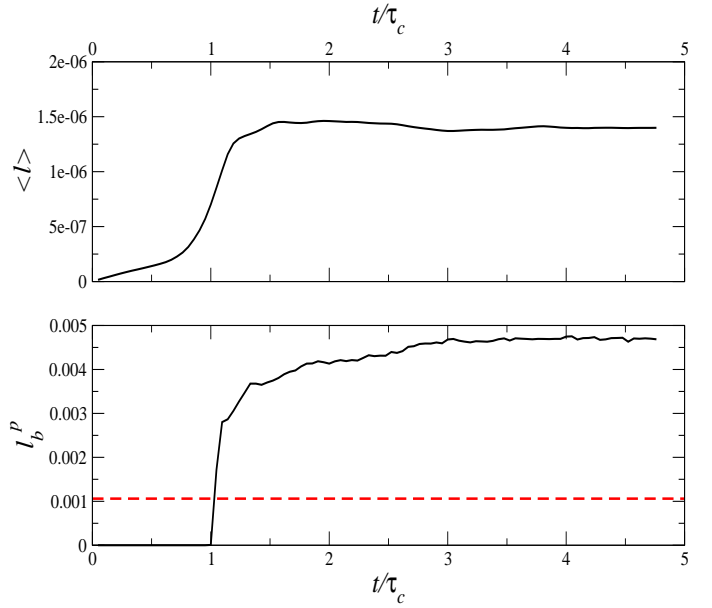


**Fig. 5.** For the case  $\alpha = 1$ , and  $N = 10^5$ , the upper panel shows the evolution of the average of the modulus of the angular momenta of bound particles (with respect to their center of mass) as a function of time. The lower panel shows the quantity in Eq. 9, and the dashed line the estimated value expected if the ejection were a random sampling of the total mass.

where  $E_p$  is (by energy conservation) the total ejected energy in the frame in which the particles are initially at rest, i.e. the sum of the kinetic energy of the center of mass of the bound mass and the kinetic energy of the ejected particles. Fig. 7 shows the same four quantities for the ellipsoidal initial conditions, as a function of  $\iota(0)$ .

Comparing these two figures, the most striking result is that there is an order of magnitude difference in the final angular momentum (as characterized by the spin parameter  $\lambda$ ) for most of the spherical initial conditions with  $\alpha \neq 0$ , and the ellipsoidal initial conditions with  $\iota(0) \neq 0$ , with a sharp interpolation between the two classes around the case  $\alpha = 0$  (which indeed is also the limit  $\iota(0) \rightarrow 0$  of the ellipsoidal initial conditions). In both figures we show also in the lower panel the final angular momentum normalized to  $L_0$ . Comparing with  $\lambda$ , we see that around  $\alpha = 0$ , where the relaxation is most violent, there is a significant difference. This arises simply from the fact that there is a considerable ejected mass, and energy, in this case: indeed the relative amplitude of the two quantities can be expressed as

$$\frac{\lambda}{L_b^p} = \left(\frac{M}{M_b}\right)^{5/2} \left(\frac{|E_b|}{|E_0|}\right)^{1/2} = \frac{(1 + f_E)^{1/2}}{(1 - f_+)^{5/2}}. \quad (10)$$

Thus the final spin includes an amplification which comes from the change in the characteristic scale of angular momentum due to the mass and energy ejection (which leads

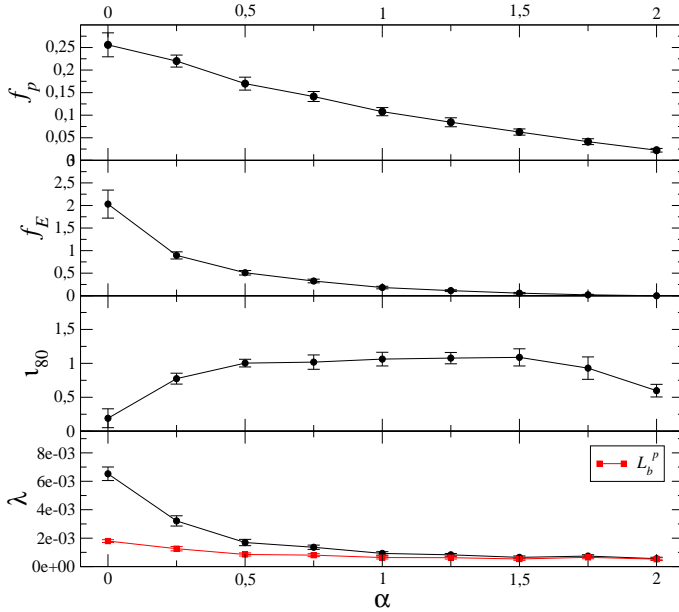


**Fig. 6.** Final values of  $f_+$ ,  $\iota_{80}$  and  $\lambda$  for the spherical initial conditions as a function of  $\alpha$ , for  $N = 10^4$ . The points are the average values for  $N_s = 20$  realizations for each  $\alpha \neq 0$ , and for 47 realizations in the case  $\alpha = 0$ ; the indicated error bar is the corresponding standard deviation  $\sigma$  (for  $\lambda$  we show the error on the mean  $\sigma/\sqrt{N_s}$ ). The lower panel also shows (red points, dashed) the angular momentum of the bound mass normalized to  $L_0$ . For the smallest values of  $\alpha$  the angular momentum generated actually decreases, but, because of the increasing mass (and energy) ejection the characteristic angular momentum of the final bound mass decreases even faster.

to a more bound, but less massive, structure than the initial condition).

It is clear, however, from the two plots that this amplification from the normalization is not the main factor explaining the much larger final angular momenta from the ellipsoidal initial conditions. Rather the main effect amplifying the spin in the ellipsoidal initial conditions compared to the spherical ones comes clearly from the essential difference in the initial conditions: the stronger initial breaking of the spherical symmetry. This initial asymmetry both leads to a more anisotropic collapse compared to that in the spherical case) and, at the same time, the ejection of a comparable amount of mass to that in the small  $\alpha$  spherical models. As described in detail in Benhaïem & Sylos Labini (2015), the particles on the stretched axis of the initial condition fall slightly later, and receive a large energy boost. Note that it is only for  $\iota_{80}(0) < 0.15$  that the final  $\iota(t)$  is linearly proportional to the initial one. Instead, for  $\iota_{80}(0) > 0.15$ , substructures form during the collapse, leading to a substantial difference in the shape of the virialized structure Benhaïem & Sylos Labini (2015). Similarly the fraction of

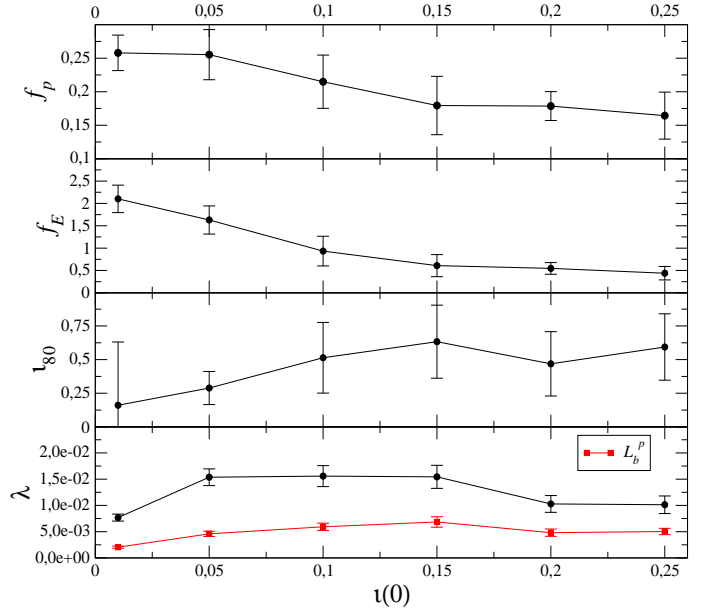


**Fig. 7.** Final values of  $f_+$ ,  $\iota_{80}$  and  $\lambda$  for ellipsoidal initial conditions, as a function of  $\iota(0)$ . The points are averages for 20 realizations, and the error bar the corresponding standard deviation (for  $\lambda$  we show the error on the mean). As in the previous figure the lower panel displays also (red points, dashed line) the final angular momentum normalized to  $L_0$ .

ejected particles decreases linearly with  $\iota_{80}(0)$  only for  $\iota_{80}(0) < 0.15$ .

Besides the angular momentum itself, the generation of a net relative motion of the center of masses of the final bound and ejected mass is also a direct measure of symmetry breaking. We would thus expect that we might find a similar trend in the final linear momentum of the ejected (or bound) particles. Shown in Fig. 8 is a plot, for all our simulations with  $N = 10^4$  particles, of both  $\lambda$  and  $\mu$ , the modulus of the “final” linear momentum of the ejected particles (equal and opposite to that of the bound mass up to a numerical precision which is smaller by several orders of magnitude in all cases.) We observe that there is indeed a clear correlation between the two quantities. Further it appears highly consistent with a roughly linear relation, as one might expect, given that they are both indirect measures of an initially small spherical symmetry breaking.

We have studied finally also the scale dependence of the normalized spin parameter defined as (Bullock et al., 2001)

$$\lambda'(r) = \frac{L_b^p(r)}{\sqrt{2GM(r)^3r}} \quad (11)$$

where  $L_b^p(r)$  is the angular momentum of bound particles with distance  $< r$  from their center of mass and  $M(r)$  is the mass enclosed in a sphere of radius  $r$ . Results for five different sets of simulations with  $\alpha = 0, 0.5, 1, 1.5, 2$  and



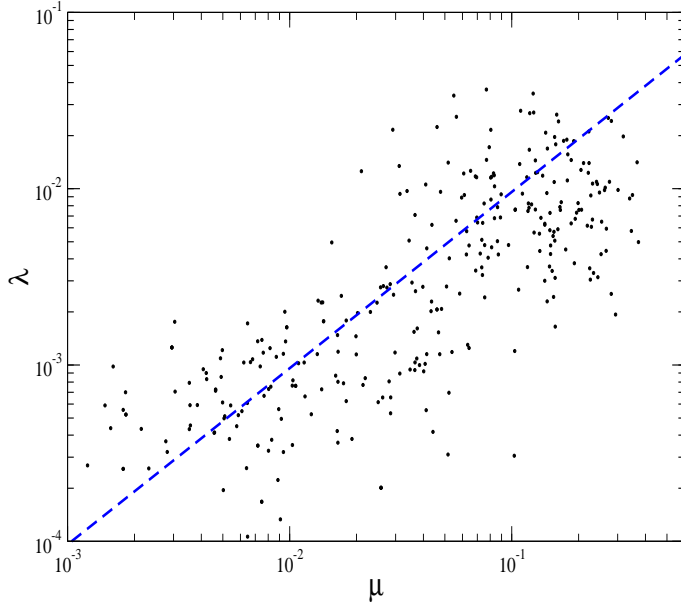


**Fig. 8.** Final spin parameter  $\lambda$ , and the modulus of final total linear momentum of the bound particles  $\mu$ , in all our (322) realizations of initial conditions (both spherical and ellipsoidal) with  $N = 10^4$ .  $\mu$  is normalized in units in which  $GM^3/R_0 = 1$ . The dashed line is  $\lambda \propto \mu$ .

$N = 10^5$  are shown in Fig. 9. The profiles are similar in all cases, but their amplitude depends on  $\alpha$  as highlighted in Fig. 6. The fact that  $\lambda'(r)$  is larger for  $\alpha = 0$  than for  $\alpha > 0$  is related to the fact orbits are slightly more radial in the former case.

### 3.6. Correlation of angular momentum with final spatial distribution

As analyzed in detail in Benhaïem & Sylos Labini (2015); Sylos Labini, Benhaïem & Joyce (2015) there is, for both classes of initial conditions, a correlation between the direction in which mass is ejected and the longest axis of both the initial condition and the final bound mass. These latter two are strongly correlated because it is the growth of the initial fluctuations breaking spherical symmetry, amplified by the mass ejection, which leads to the final spatial asymmetry. The fact that the ejection of mass is amplified along these same directions is because they are the particles which fall latest and pick up as a result a large energy kick. Given that we have seen that most of the final angular momentum is generated at the time of ejection, we would expect that it would preferably be aligned orthogonal to the preferential axis for ejection.

Shown in Figs. 10 and 11 are histograms, for 20 realizations of each indicated initial condition, of the modulus of the cosine of the angle between the final angular momentum of the bound mass,  $\mathbf{L}_b^p$ , and the eigenvector corresponding to the longest axis of the final bound mass (blank

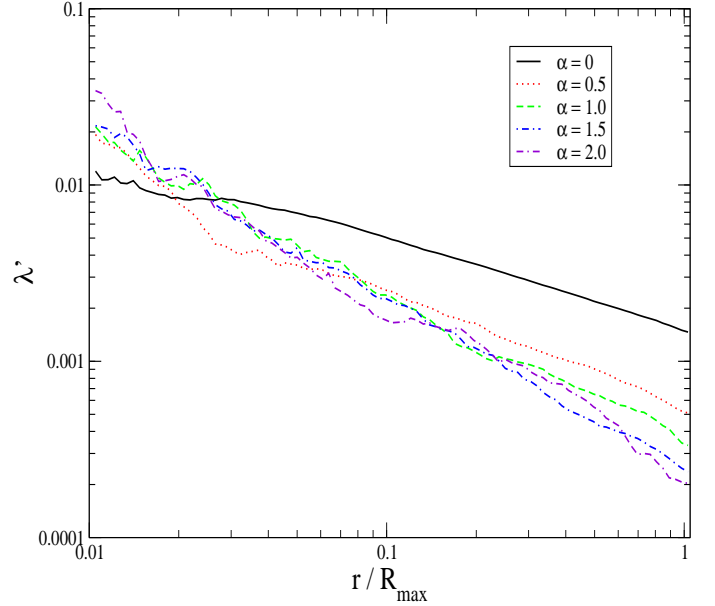


**Fig. 9.** Spin parameter  $\lambda'(r)$  (see Eq. 11), averaged over 20 realizations, for  $\alpha = 0, 0.5, 1, 1.5, 2$  and  $N = 10^5$ . The distance is normalized to the structure size  $R_{max}$ .

histograms), and the final ejected mass (filled histograms). For the ellipsoidal initial conditions - which very strongly single out an initial preferred axis which remains strongly correlated with the final longest axis - the anticipated correlation is very clearly present. In the spherical initial conditions, the correlation is weaker but nevertheless visible, except perhaps in the case  $\alpha = 0$ . Indeed in this latter case, as discussed in Sylos Labini, Benhaïem & Joyce (2015), the symmetry breaking in the final state is in fact much weaker, and the correlation between the final and initial asymmetry likewise. This is a result of the fact that in this case, in which the fall time of all particles is the same in the limit  $N \rightarrow \infty$ , there is a much weaker correlation between the initial radial position of a particle and the energy change it undergoes in the violent collapse.

### 3.7. Dependence on $N$

The  $N$  dependence of the angular momentum generated by mass ejection has been explored in Worrakitpoonpon (2015) for the case  $\alpha = 0$ , and evidence for a monotonic decrease  $\sim N^{-\beta}$ , with a best fit around  $\beta = 1/3$ , was found. Inspection of the results we have reported above, for simulations with  $N = 10^4$  and  $N = 10^5$ , are consistent with this finding for this case, while for initial conditions with  $\alpha > 0$ , an apparent decrease of the average  $L_p^b$  as  $N$  grows is also observed. To explore this further, we have performed a more detailed study of the case  $\alpha = 1$ , performing a larger number of simulations for a greater number of values of  $N$  in the range  $10^3$  to  $10^5$ . We have in this case also evolved each simulation for a longer time to

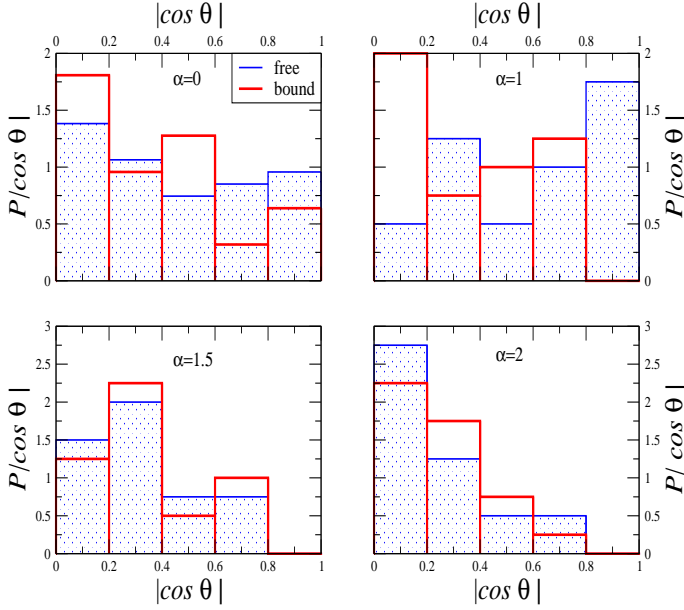


**Fig. 10.** Histogram of the cosine of the angle, well after the collapse, between  $L_b^p$  and the eigenvector corresponding to the longest principal axis of the final bound mass (blank histograms), and of the ejected mass (filled histograms), for 20 realizations of spherical initial conditions for different  $\alpha$  indicated in the caption.

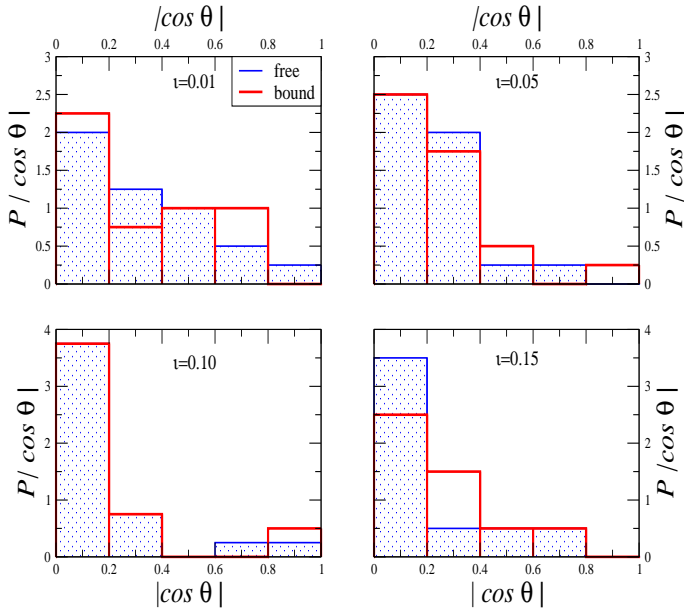


**Fig. 11.** Pdf of the cosine of the angle, well after the collapse, between  $L_b^p$  and the eigenvector corresponding to the longest principal axis of the final bound (blank histograms), and of the ejected mass (filled histograms), for 20 realizations of ellipsoidal initial conditions for different  $\iota(0)$  indicated in the caption.

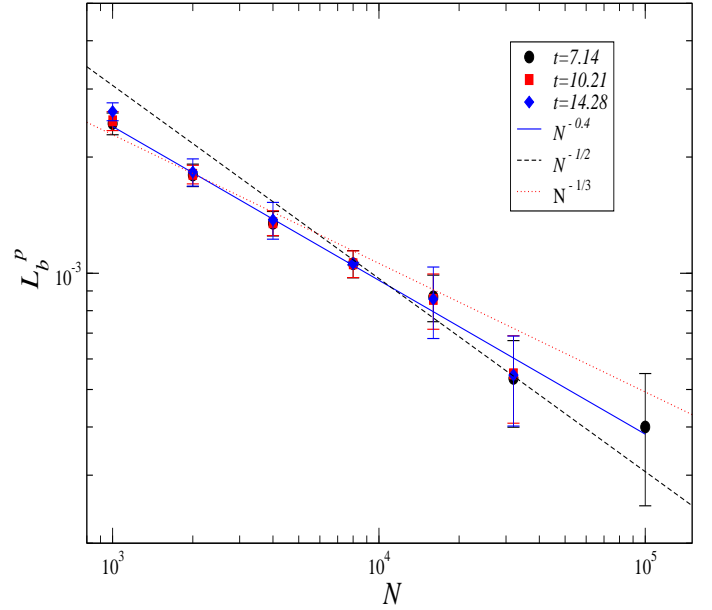


**Fig. 12.** Logarithm of the final angular momentum of bound virialized mass  $L_b^p$  (in units of  $L_0$ ) as a function of particle number  $N$ , for spherical initial conditions with  $\alpha = 1$ . The point for the cases  $N = 10^5$  correspond to the results reported above, at  $t = 5$ , while for the other  $N$  there is data at three times, extending to  $t \approx 14$ . Each point is an average over  $M$  realizations, with  $M = 90$  for  $N = 1000$ ,  $M = 50$  for  $N = 2000$ ,  $M = 40$  for  $N = 4000$ ,  $M = 30$  for  $N = 8000$ ,  $M = 6$  for  $N = 16000$ ,  $M = 4$  for  $N = 32000$ , and  $M = 4$  for  $N = 10^5$ . The error bars indicate the corresponding estimated error on the mean. The continuous line ( $\propto N^{-0.4}$ ) is a best-fit to the data, while the dashed lines corresponds to  $N^{-1/2}$  and  $N^{-1/3}$ .

study the stability of our “final” measures of the different quantities, and to check for the possible role of finite  $N$  effects.

Shown in Fig. 12 is the result for the measured angular momentum  $L_b^p$ , at the indicated times, in a series of simulations for the different indicated values of  $N$ . As anticipated, in the cases where different (and longer) times have been analyzed the measured angular momentum shows no significant dependence on the time: after the few dynamical time there is negligible interaction between the ejected and bound mass and the angular momentum of each are constant. As a function of  $N$ , on the other hand, there is a clear monotonic decrease, well fitted by a power law dependence,  $L_b^p \propto N^{-\gamma}$ , with  $\gamma \approx 0.4$ . The dashed lines indicate, for comparison, the behaviors  $N^{-1/2}$  and  $N^{-1/3}$ .

Shown in Fig. 13 is the result for the same data as in the previous figure, and for the different  $N$  shown, for the flatness ratio  $\iota_{80}$ . In contrast we see in this case that the value measured, for all but the largest value of  $N$ , shows visible dependence on time. More specifically the bound mass evolves towards a more spherical distribution

in time, at a rate which is clearly faster for the smaller  $N$ . Such an  $N$  dependence of the time scale of the evolution of the virialized structure is clearly qualitatively coherent with collisional relaxation, and indeed a quantitative analysis of such behavior from similar initial conditions in Theis & Spurzem (1999) shows that the timescale of this evolution is indeed in agreement with that predicted by two-body collisionality. At the very largest  $N$ , on the other hand, the result appears to converge to a time independent value. In the small range of (larger)  $N$  in which this time-dependence due to two body collisionality is small the final value appears to be consistent with an  $N$ -independent behavior, but clearly extrapolation to larger  $N$  would be needed to reach a firmer conclusion. We underline that, in contrast, we do not have this problem for the determination above of the scaling with  $N$  of  $L_p^b$  as this quantity is essentially frozen, as we have seen, at about  $t \approx 2$ , and thus not modified by the two body collisionality at longer times. We note that Joyce, Marcos & Sylos Labini (2009) report tests for collisionality during the collapse phase, for the very extreme case of a flat ( $\alpha = 0$ ) profile, and conclude, in line with the study of Aarseth, Lin & Papaloizou (1988), that for  $N > 10^3$  collisional effects during the collapse phase are indeed negligible. This result, consistent with theoretical prediction for the collisional time scale, is borne out by the observation that the evolution of the macroscopic features of the collapse — potential energy, viral ratio, size of structure, and in particular the fraction of the mass ejected — are stable when  $N$  increases, and likewise when the gravitational force softening is varied, provided it is sufficiently small to resolve the mean gravitational field.

Given that, as we have emphasized, the breaking of spherical symmetry in the initial conditions is due to finite  $N$  fluctuations, the fact we find that the final angular momentum  $L_p^b$  decreases as  $N$  increases, and in principle goes to zero as  $N \rightarrow \infty$ , is what one would naively expect. A similar decrease in amplitude, with an exponent of about the same value, has been observed for the case  $\alpha = 0$  in Worrakitpoonpon (2015). In our simulations of initial conditions from elliptical conditions we have not been able to detect, within the significant scatter of different realizations at given  $N$ , a clear trend for  $L_p^b$  to decrease as  $N$  increases. This is probably because of a weaker  $N$  dependence in this case, as the spherical symmetry is “mostly” broken by  $\iota(0) \neq 0$  which does not depend on  $N$ . In contrast the lack of evidence for any  $N$  dependence in the final  $\iota$  — once  $N$  is sufficiently large so that collisional relaxation plays no role on the time scales probed — may be indicative of the true physical behavior: in the limit of exact spherical symmetry of an exactly cold system, it is expected that symmetry be broken due to so-called radial orbit instability. In future work we will study more fully the  $N$  dependence of both the breaking of symmetry, and that of the angular momentum of the ejected particles, and their connection to one another.

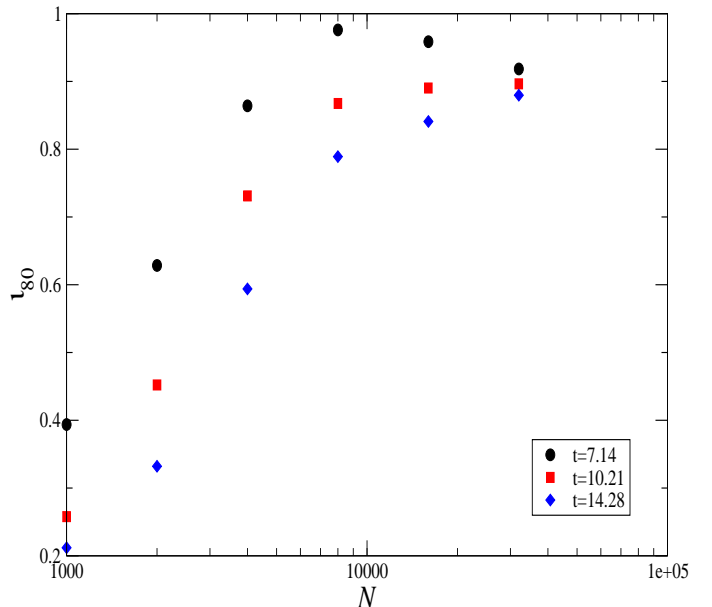


**Fig. 13.** Flatness ratio  $\iota_{80}$  as a function of particle number  $N$ , for the same simulations in the previous figure ( $\alpha = 1$ ) for the indicated values of  $N$ . For this quantity the observed  $N$  dependence is due to two body relaxation which make the system evolve in time towards a more spherical quasi-equilibrium.

#### 4. Discussion and conclusions

The origin of the angular momentum in astrophysical structures — notably that measured observationally in galaxies — is a fascinating open problem in astrophysics and cosmology. In this article we have discussed and studied a way, different to commonly considered ones such as tidal torques, in which angular momentum can be generated by self-gravity only. It can occur in principle for initial conditions which evolve sufficiently violently — with large variations of the gravitational mean field — so that mass is ejected during relaxation towards a virialized state. We have shown using numerical simulations for two simple broad classes of initial conditions of this kind that significant angular momentum can indeed be generated in this way, orders of magnitude larger in most cases than the angular momentum error due to numerics.

We have, for illustrative purposes, and for simplicity, considered initial conditions very close to spherical symmetry. Indeed in all our initial conditions rotational symmetry is only broken fully by the Poissonian density fluctuations associated with the finite number of particles. Interestingly we find that, despite the “artificiality” of our initial conditions, which are not motivated by any detailed specific physical model, we obtain angular momenta which are of comparable size — only smaller by a factor of two in some cases — than those typically estimated for galaxies. Indeed we have obtained values of the normalized “spin parameter” up to  $\lambda \sim 0.02$ , while, for ex-

ample, Hernandez et al. (2007) have estimated its average value in the 11597 spirals and elliptical galaxies observed by the Sloan Digital Sky Survey to be  $\lambda_0 = 0.04 \pm 0.005$ , (and standard deviation  $\sigma_\lambda = 0.51 \pm 0.05$ ). While obviously galaxy formation in particular involves much more complicated non-gravitational processes than described by the simple models we have considered here, and further our specific initial conditions are quite ad hoc (and not directly motivated by a cosmological model) it is intriguing that the order of magnitude of the values we obtain are in line with those observed.

We note that studies of dark matter halos in cosmological N-body simulations (see e.g. Vitvitska et al. (2002); Bullock et al. (2001); Bett et al. (2007)) give rise to similar values of spin parameter ( $\lambda \approx 0.04$ ), i.e. of the same order as those observed in elliptical galaxies, and as those we find in our simulations in certain cases. As dark matter halos of standard cold dark matter cosmologies form through a hierarchical process rather than in the kind of monolithic collapse we have studied, the mechanism we have studied has likely no relevance in this particular context. Indeed it is the strong violence of the collapse leading to mass ejection which is crucial, and the formation of halos in a cold dark matter cosmology setting is not of this kind. Nevertheless, as discussed in Carucci et al. (2014); Samsing (2015), significant mass ejection can occur in a cosmological setting when halos merge and it would be interesting to investigate whether this could lead also to generation of angular momentum at a significant level, compared to the processes of mass accretion, for example, which has been argued in Vitvitska et al. (2002) to account for the spin of dark matter halos.

Just as in cosmological simulations we underline that we are simulating essentially the collisionless regime of the gravitational dynamics (apart from the two body collisional effects which we observed to be present at longer times in smaller  $N$  simulations). In so far as this is true, the particle number  $N$  is relevant, in principle, in the properties of the final state just because it fixes the amplitude of the initial fluctuations. Indeed these fluctuations are, for our initial conditions in this paper, simply Poissonian, and thus their amplitude at any scale (and all their statistical properties) are regulated by this single parameter. Alternatively one could consider setting up an initial particle with the same average density profile but with statistical fluctuations with non-trivial correlation, described for example by non-trivial two-point correlation properties. In this case one could then in principle vary  $N$  while keeping the relevant fluctuations fixed and obtain results independent of  $N$ . As the fluctuations play an essential role in the symmetry breaking, we expect that the detailed nature of such initial fluctuations may have an impact on the properties of the final structure. We postpone a detailed study of this interesting issue to future work. We will also explore whether cold but more irregular/clumpy initial conditions can produce values of the spin of the order of magnitude to those observed for galaxies. Further we will explore whether the kind of correlation we have

discussed briefly in the last part of the paper — between the shape of the asymmetric virialized structure and its angular momentum — could be used to find observational evidence for or against the role of very violent relaxation in generating the structure of galaxies.

Numerical simulations have been run on the Cineca PLX cluster (project ISCRA BSS-GC), and on the HPC resources of The Institute for Scientific Computing and Simulation financed by Region Ile de France and the project Equip@Meso (reference ANR-10-EQPX- 29-01) overseen by the French National Research Agency (ANR) as part of the Investissements d’Avenir program.

## References

- Aarseth S., Lin D., Papaloizou J., 1988, *Astrophys. J.*, 324, 288
- Aguilar L., Merritt D., 1990, *Astrophys. J.*, 354, 73
- Antonov V. A., 1961, *Soviet Ast.*, 4, 859
- Barnes E. I., Lanzel P. A., Williams L. L. R., 2009, *Astrophys. J.*, 704, 372
- Bellazzini M., Bragaglia A., Carretta E., Gratton R. G., Lucatello S., Catanzaro G., Leone F., 2012, *Astron.Astrophys.*, 538, A18
- Benhaïem D., Sylos Labini F., 2015, *Mon.Not.R.Astron.Soc.*, 448, 2634
- Bett P., Eke V., Frenk C. S., Jenkins A., Helly J., Navarro J., 2007, *Monthly Notices of the Royal Astronomical Society*, 376, 215
- Boily C., Athanassoula E., Kroupa P., 2002, *Mon. Not. R. Astr. Soc.*, 332, 971
- Boily C. M., Athanassoula E., 2006, *Mon. Not. R. Astr. Soc.*, 369, 608
- Bullock J. S., Dekel A., Kolatt T. S., Kravtsov A. V., Klypin A. A., Porciani C., Primack J. R., 2001, *Astrophys.J.*, 555, 240
- Carucci I. P., Sparre M., Hansen S. H., Joyce M., 2014, *JCAP*, 6, 57
- Fridman A. M., Polyachenko V. L. 1984, *Physics of gravitating systems. I. Equilibrium and stability*. Springer Verlag
- Hénault-Brunet V. et al., 2012, *Astron.Astrophys.*, 545, L1
- Henon M., 1973, *Ann. Astrophys.*, 24, 229
- Hernandez X., Park C., Cervantes-Sodi B., Choi Y.-Y., 2007, *Monthly Notices of the Royal Astronomical Society*, 375, 163
- Joyce M., Marcos B., Sylos Labini F., 2009, *Mon. Not. R. Astron. Soc.*, 397, 775
- Joyce M., Sylos Labini F., 2013, *Mon.Not.R.Astr.Soc.*, 429, 1088
- Kacharov N. et al., 2014, *Astron.Astrophys.*, 567, A69
- Knebe A., Power C., 2008, *Astrophys.J.*, 678, 621
- Lin C. C., Mestel L., Shu F. H., 1965, *Astrophys. J.*, 142, 1431
- Merritt D., Aguilar L. A., 1985, *Mon. Not. R. Ast. Soc.*, 217, 787



- Peebles P. J. E., 1969, *Astrophys.J.*, 155, 393
- Romanowsky A. J., Fall S. M., 2012, *Astrophys. J. Supp.*, 203, 17
- Samsing J., 2015, *Astrophys.J.*, 799, 145
- Springel V., 2005, *Mon. Not. R. Ast. Soc.*, 364, 1105
- Sylos Labini F., 2012, *Mon. Not. R. Astron. Soc.*, 423, 1610
- Sylos Labini F., 2013, *Mon. Not. R. Astron. Soc.*, 429, 679
- Sylos Labini F., 2013, *Astronomy & Astrophysics*, 552, A36
- Sylos Labini F., Benhaïem D., Joyce M., 2015, *Mon.Not.R.Astron.Soc.*, 449, 4458
- Theis C., Spurzem R., 1999, *Astron. Astrophys.*, 341, 361
- van Albada T., 1982, *Mon. Not. R. Astr. Soc.*, 201, 939
- Vitvitska M., Klypin A. A., Kravtsov A. V., Wechsler R. H., Primack J. R., Bullock J. S., 2002, *The Astrophysical Journal*, 581, 799
- Worrakitpoonpon T., 2015, *Mon. Not. R. Astr. Soc.*, 466, 1335